Dalton Transactions

PAPER

View Article Online
View Journal | View Issue

Exalted photocatalytic activity of tetragonal $BiVO_4$ by Er^{3+} doping through a luminescence cooperative mechanism†

Cite this: *Dalton Trans.*, 2014, **43**, 311

Sergio Obregón,[a,b] Soo W. Lee[b] and Gerardo Colón*[a]

Received 16th July 2013,
Accepted 11th September 2013

DOI: 10.1039/c3dt51923f

www.rsc.org/dalton

Er-doped $BiVO_4$ are synthesized by means of a surfactant free microwave assisted hydrothermal method having good photoactivities under sun-like excitation for the degradation of methylene blue. From the structural and morphological characterization, it has been stated that the presence of Er^{3+} induces a slight stabilization of the tetragonal phase, probably due to its incorporation in the $BiVO_4$ lattice. The best photocatalytic performances were attained for the samples with Er^{3+} content higher than 3 at%. The occurrence of the Er^{3+} doped tetragonal $BiVO_4$ clearly induces higher photocatalytic activities. The existence of a luminescence process has been related with the enhanced photoactivity observed.

Introduction

Heterogeneous photocatalysis is regarded as a green route to afford pollutant degradation. Moreover, other different green chemistry reactions such as water or CO_2 photoreduction to produce H_2 or biofuels are now gaining interest. In this sense, the utilization of solar light as efficiently as possible has been largely pursued. Towards this aim, different approaches have been traditionally followed, based in all cases on the visible light photon absorption improvement. This way, the photonic efficiency will be enhanced by simply increasing the number of useful photons available. For this scope, the modification of TiO_2 by cation doping has been extensively reported with controversial results in certain cases.[1] Other strategies recently reported involve the development of novel alternative materials to traditional TiO_2 capable of using sunlight as a green energy source.[2]

In this sense, bismuth vanadate has been found to be a promising candidate used for organic contaminants decomposition as well as in CO_2 reduction under visible-light irradiation.[3–7] $BiVO_4$ appears in three main crystalline phases: monoclinic, tetragonal zircon, and tetragonal scheelite. Among the above three crystal phases, monoclinic $BiVO_4$ (m-$BiVO_4$) is the best visible-light-driven photocatalyst due to its lower band gap value (*ca.* 2.4 eV), while the photocatalytic activity of tetragonal $BiVO_4$ (t-$BiVO_4$) was reported to be negligible.[8–11] For this reason, different synthetic methods have been recently proposed for obtaining the photoactive monoclinic phase.[12–14]

A novel challenging composite configuration would consist of the assembly of the photocatalytic material with a luminescence material.[2] Within this novel configuration, the improvement is reached by increasing the number of incoming photons with adequate energy which can be absorbed by the photocatalyst. Among various up-converting nanomaterials, Er^{3+} constitutes an interesting option for this purpose which could be excited by visible-light or NIR, showing luminescence in the visible and ultraviolet regions.[15,16] In a recent paper, we described the assembly of TiO_2 with such up-converting doping cations.[17] From those results, we proposed that the presence of Er^{3+} doping into TiO_2 as host matrix favors a double electronic and luminescence mechanism, under UV and NIR excitation respectively.

Experimental details

The $BiVO_4$ samples were prepared by a microwave-assisted hydrothermal method. Firstly, 5 mmol of $Bi(NO_3)_3{\cdot}5H_2O$ (Sigma-Aldrich, ≥98.0%) and stoichiometric amounts of $Er(NO_3)_3$ (from 0.25 to 4 at%) were dissolved in 10 mL of glacial acetic acid at room temperature. A second aqueous solution was prepared by dissolving the corresponding stoichiometric amount of NH_4VO_3 (Sigma-Aldrich, ≥99.0%) in 60 mL of hot distilled water. Afterwards, the ammonium metavanadate solution was added to the bismuth nitrate

[a]*Instituto de Ciencia de Materiales de Sevilla, Centro Mixto CSIC-Universidad de Sevilla, Américo Vespucio, 49, 41092 Sevilla, Spain. E-mail: gcolon@icmse.csic.es; Fax: +34954460665; Tel: +34954489536*

[b]*Department of Materials Engineering, Sun Moon University, Galsan-Ri, Tangjung-Myon, Asan, 336-708, South Korea*

† Electronic supplementary information (ESI) available: Preparation and photocatalytic activity of $BiVO_4$ by the mw-assisted hydrothermal method. See DOI: 10.1039/c3dt51923f

aqueous solution and the process was accompanied with vigorous stirring. The pH of the obtained suspension was adjusted to 9.0 by adding concentrated NH_4OH (13 mol L^{-1}). The slurry was transferred to a Teflon vessel and heated under microwave irradiation using a microwave reactor (model MWO-1000S, EYELA; Japan). The temperature was fixed at 140 °C with a maximum variable power of 195 W for 30 minutes (being the optimum microwave treatment time, see ESI†). The obtained precipitate was then cooled until room temperature, filtered and repeatedly washed and dried overnight at 120 °C. Afterwards, thus obtained samples were submitted to a further calcination treatment at 300 °C for 2 h. A reference tetragonal $BiVO_4$ sample was prepared by following the synthetic route above described but using triethylamine (TEA) as a precipitating agent.

BET surface area and porosity measurements were carried out by N_2 adsorption at 77 K using a Micromeritics 2010 instrument.

The structural characterization was carried out by X-ray powder diffraction using a Rigaku, RINT-2200 diffractometer with CuKα radiation. X-ray diffraction data of the samples were registered between 10° and 70° (2θ) with a scanning velocity of 0.05° s^{-1}.

Micro-Raman measurements were performed using a LabRAM Jobin Yvon spectrometer equipped with a microscope. Laser radiation (λ = 532 nm) was used as an excitation source at 5 mW. All measurements were recorded under the same conditions (2 s of integration time and 30 accumulations) using a 100× magnification objective and a 125 mm pinhole.

Erbium content was measured by micro-XRF elemental analysis (EDAX Eagle III). For the quantitative analysis, an erbium calibration curve was previously constructed from different Er–$BiVO_4$ reference samples.

The morphology of samples was followed by means of field emission-SEM (Hitachi S 4800). The samples were dispersed in ethanol using an ultrasonicator and dropped on a copper grid.

The UV diffuse reflectance spectra were measured using an UV-vis spectrophotometer equipped with an integrating sphere (JASCO V-570). The reference sample used was a $BaSO_4$ coated standard pattern.

The excitation and emission spectra of the catalysts were recorded at ambient temperature using a Horiba Jobin-Yvon Fluorolog3 spectrofluorometer operating in the front face mode with a 1.5 nm slit. The UC optical measurements were performed for powdered pressed samples using a Jenoptik laser diode source at 980 nm. The resulting luminescence was dispersed by using an ARC Spectrapro 500-I monochromator and then detected with a photomultiplier tube.

The photocatalytic activity of the samples was tested by means of degradation of methylene blue dye under simulated solar conditions. In a typical procedure, 0.05 g of photocatalyst was placed in a batch reactor containing 50 mL of methylene blue whose initial concentration was 10 mg L^{-1}. The suspension was maintained under dark conditions for 15 min in order to achieve the adsorption–desorption equilibrium of the dye on the photocatalyst surface. Afterwards, the suspension was irradiated with simulated solar light by means of a solar simulator PEC-L01, Peccell equipped with a 150 W Xe lamp (150 W cm^{-2}, 1.5 sun). Samples of 1 mL were taken at given time intervals and the photocatalyst was separated using a nylon filter. The concentrations were monitored by checking the absorption spectrum of each sample through its absorption band maximum (664 nm) using an UV-Vis spectrophotometer (Mecasys Optizen 2120UV).

Results and discussion

The preparation of $BiVO_4$ by the mw-assisted hydrothermal method leads to the monoclinic phase structure (*PDF* 14-0688) in all cases (see ESI†). Upon Er^{3+} doping, it can be observed that the monoclinic phase is attained for dopant content below 2 at%. For higher Er contents, a mixture of the tetragonal phase arises (*PDF* 14-0133), being the main crystalline phase for systems with Er^{3+} content higher than 3 at%. This tetragonal stabilization by lanthanide doping has been similarly described by other authors.[18,19] Since the tetragonal phase was denoted as the low temperature structure of $BiVO_4$, the occurrence of such doping ions in the $BiVO_4$ structure seems to retard the monoclinic appearance.[20] As can be observed from XRD pattern evolution, this effect is evident for Er^{3+} contents higher than 3 at%. No traces of Er_2O_3 were found even for samples with higher doping loading (Fig. 1). In this sense, the effectiveness of erbium doping was stated by XRF (Table 1). Thus, obtained Er^{3+} content by elemental analysis adequately fits with nominal values.

From Rietveld analysis it can be pointed out that at lower Er^{3+}, the m-$BiVO_4$ structure is not significantly affected (Table 1).

The cell volume of the monoclinic structure slightly grows as the Er^{3+} content increases. From this behaviour, it can be inferred that in spite of the lower ionic radius of Er^{3+} *vs.* Bi^{3+} (103 pm and 117 pm respectively), the substitution of Bi^{3+} by

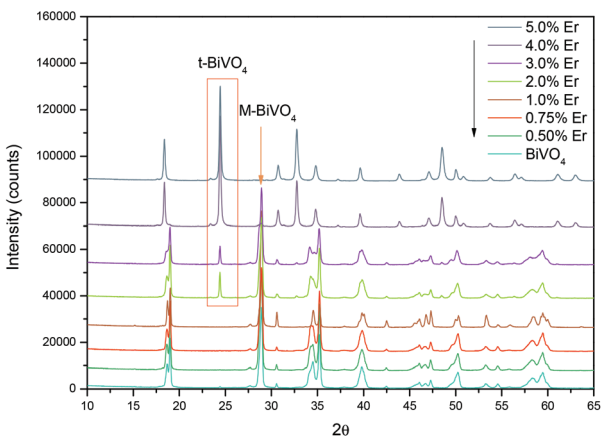

Fig. 1 X-ray diffraction patterns for Er^{3+}–$BiVO_4$ catalysts obtained by mw-hydrothermal synthesis at 140 °C for 30 min.

Table 1 Structural and surface characterization of Er^{3+}–$BiVO_4$ systems

Samples	BET ($m^2\ g^{-1}$)	Tetragonal (%)	Cell volume (Å^3)		Band gap (eV)	Er[a] (at%)
			M	*T*		
$BiVO_4$	1.0	0	311.08	—	2.4	—
Er 0.5%	1.4	0	311.14	—	2.4	—
Er 0.75%	1.0	0	311.20	—	2.4	—
Er 1.0%	1.3	0	311.15	—	2.4	0.9
Er 2.0%	1.0	2	310.95	343.95	2.4	2.4
Er 3.0%	1.0	4	310.72	343.68	2.4	3.3
Er 4.0%	5.1	96	—	434.38	2.4/2.9	4.6
Er 5.0%	4.0	100	—	343.05	2.9	5.2

[a] Measured by X-ray fluorescence.

Er^{3+} ions is not taking place. Therefore, Er^{3+} would be placed interstitially causing this small cell expansion. When the tetragonal phase is present, Er^{3+} produces a clear diminution of the cell volume (Table 1). Such a volume contraction could indicate the effective substitution of Bi^{3+} by Er^{3+} in the tetragonal structure.

In accordance with the literature, the surface areas obtained for all samples are significantly low (Table 1). However, systems with a tetragonal phase show slight increase in surface areas. At the same time, two clear absorption edges can be noticed when the tetragonal phase in present, leading to 2.4 eV and 2.9 eV band gap values for the monoclinic and tetragonal phases, respectively (Table 1).

The Raman spectra of this series also support the presence of a single monoclinic phase at lower Er^{3+} content (Fig. 2). For higher lanthanide loading, strong luminescence bands correspond to the fluorescence emission of Er^{3+} due to the excitation of green laser (532 nm) (Fig. 2a). It is worth noting that the presence of strong luminescence is correlated with the occurrence of the tetragonal structure. It can be inferred that when Er^{3+} is substituting Bi^{3+} in the vanadate matrix, the luminescence emission occurs. In this sense, it has been reported that trivalent metal orthovanadates show excellent performances as matrices for luminescent lanthanides due to efficient energy

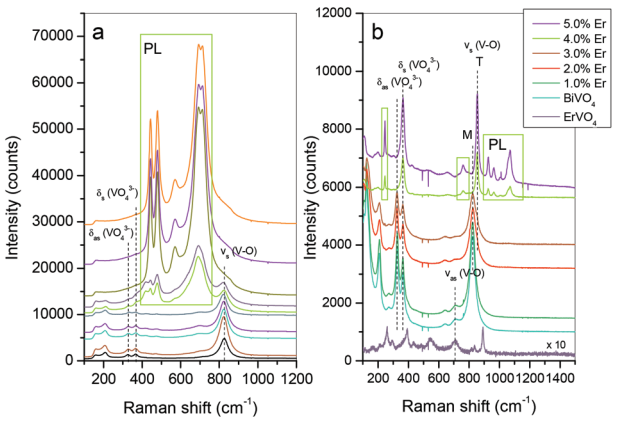

Fig. 2 (a) Raman spectra for Er^{3+}–$BiVO_4$ systems under green laser excitation (532 nm); (b) under red laser excitation (780). Photoluminescence bands are denoted in the square as PL.

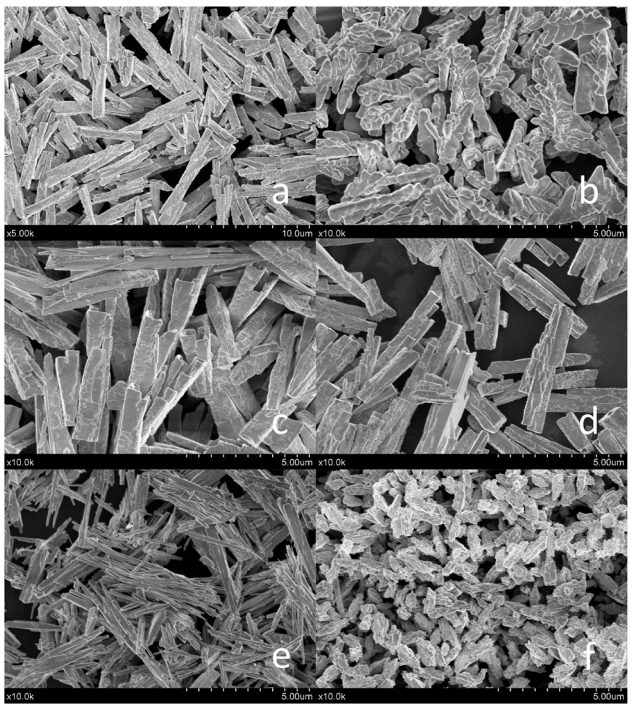

Fig. 3 SEM images for Er–$BiVO_4$ systems with different Er contents: (a) bare $BiVO_4$; (b) 1 at%; (c) 2 at%; (d) 3 at%; (e) 4 at%; (f) 5 at%.

transfer (ET) from the VO_4^{3-} absorption to the excited states of the activators (Ln^{3+}).[21]

The Raman spectra registered by 780 nm laser excitation (Fig. 2b) clearly denote the monoclinic to tetragonal transition observed by ν_s (V–O) band shift and the disappearance of the δ (VO_4^{3-}) doublet of the monoclinic phase.[10] In this case, small luminescence bands from Er^{3+} excitation by red laser can also be observed.

The morphology of $BiVO_4$ has been extensively reported to be dependent on the preparation route.[22] In our case, bare $BiVO_4$ shows a rod-like morphology (Fig. 3a).

Such morphology leads to the extinction of the (040) diffraction line and a notable exaltation of diffraction lines corresponding to the planes (110) and (002), as was observed in the XRD pattern (Fig. 1).

As Er^{3+} is incorporated, the length of these rods seems to diminish (Fig. 3b–d). When tetragonal phase appears, a clear change in the morphology is observed and particles exhibit a needle-like structure. Thus, for the highest Er-doped system the acicular morphology has almost disappeared (Fig. 3e). The slight increase in the surface area could therefore be correlated with this change in the morphology and the diminution of particle size. Such evolution is directly associated with the incorporation of Er^{3+} and the subsequent phase transformation from monoclinic to tetragonal.

In Fig. 4 we show the photocatalytic activity of the studied systems. It is worth noting that the preparation of $BiVO_4$ by the mw-assisted hydrothermal method leads to higher photoactivity with respect to that prepared by the simple coprecipitation method. Moreover, the incorporation of Er^{3+} also leads to a

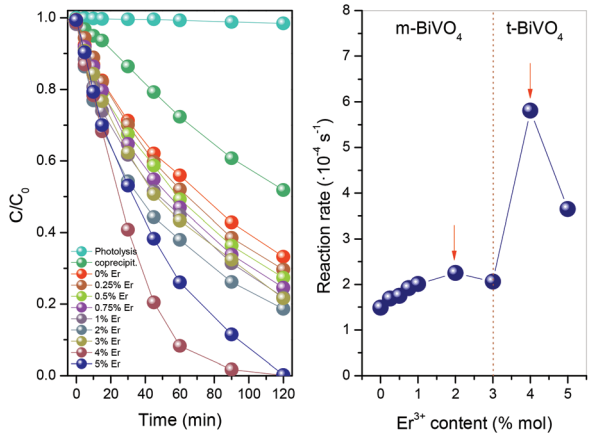

Fig. 4 (a) Evolution of *MB* C/C_0 with irradiation time and (b) evolution of calculated reaction rates for different Er content.

slight progressive enhancement till 2 at% content. This improvement could be described in terms of classical doping theory in which dopant would help the charge separation till its concentration is detrimental and promote the recombination process.[23] No luminescence emission is observed for these samples. Then, the appearance of the tetragonal phase significantly improves the photocatalytic performance of systems.

Thus, for Er^{3+} content higher than 3 at%, a drastic increase in the reaction rate is observed (Fig. 4). The optimum photoactivity was attained for systems with 4 at%, being four times higher than that corresponding to bare $BiVO_4$. It is worth noting that for such photocatalysts the tetragonal phase is mainly present (96%).

In order to elucidate the effect of Er^{3+} in this t-$BiVO_4$, we have prepared undoped t-$BiVO_4$ by a similar mw-assisted hydrothermal method. The sample obtained shows a predominant tetragonal phase (95%), presents a bar-like morphology and a surface area of 4 $m^2\ g^{-1}$ (Fig. 5). Taking into account these structural and surface features, this reference system can be directly compared to Er–$BiVO_4$ (4 at%). The *MB* degradation reaction rate obtained for this t-$BiVO_4$ is $3.0 \times 10^{-4}\ s^{-1}$. There exists a slight enhancement in the photoactivity with respect to undoped m-$BiVO_4$ ($1.5 \times 10^{-4}\ s^{-1}$). Such an improvement could be explained by considering the higher surface area of t-$BiVO_4$ and perhaps the presence of the small amount of the monoclinic phase (5%). Indeed, the presence of a monoclinic–tetragonal heterojunction was recently reported and exhibits better photocatalytic performance. Thus, Fan *et al.* reported that the particular m–t heterostructured $BiVO_4$ is expected to promote the separation of photoinduced electron–hole pairs.[24,25] In spite of this, the exalted performance of Er-doped t-$BiVO_4$ ($6.0 \times 10^{-4}\ s^{-1}$) with respect to the t-$BiVO_4$ ($3.0 \times 10^{-4}\ s^{-1}$) system cannot be attributed only to a surface area contribution or the presence of a small amount of monoclinic phase. Indeed, much research has shown that the surface area would play a key role in the final photocatalytic performance. As is widely reported, this is not the case for $BiVO_4$ systems, for which structural features are the controlling parameters.[26,27]

In a recent study, we have proposed the Y^{3+} doping of $BiVO_4$.[28] In that paper, we stated that the incorporation of yttrium at loading higher than 3 at% into the $BiVO_4$ structure leads to a clear stabilization of the tetragonal phase and the increase of the surface area. However, for doping concentrations higher than 3 at% the photoactivities tend to decay. Indeed, this is the evolution of Er–$BiVO_4$ for doping levels higher than 2 at%, just before tetragonal phase appears. This behaviour could be attributed to a detrimental effect of dopant concentration by increasing the recombination processes. All these facts would indicate that erbium doping would affect the

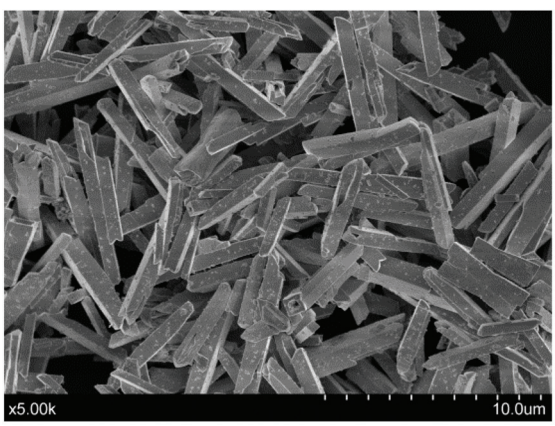

t-$BiVO_4$	BET (m^2/g)	Band gap (eV)	Cell volume (Å^3)	Reaction rate (s^{-1})
	4.2	2.86	344.6	$3.0 \cdot 10^{-4}$

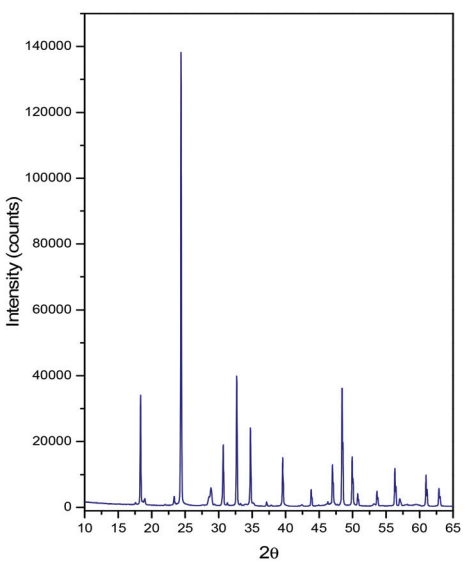

Fig. 5 Characterization summary of undoped t-$BiVO_4$.

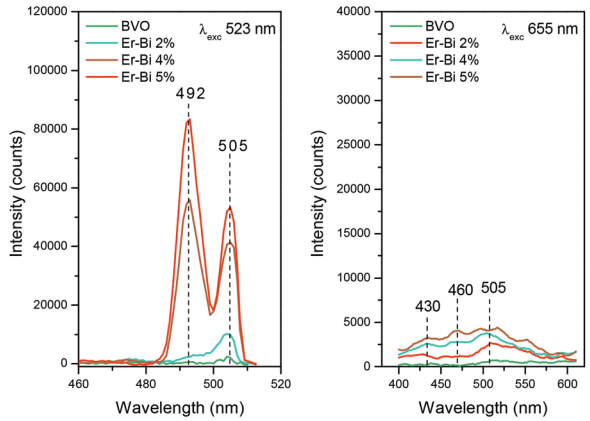

Fig. 6 Photoluminescence spectra for different Er^{3+} doped systems upon excitation at 523 nm and 655 nm.

reaction mechanism in a different particular way when the tetragonal phase is present. On this basis, and considering the developed luminescence effect observed for Er-doped t-$BiVO_4$ a cooperative mechanism could be envisaged.

Lower photoactivities reported in the literature for t-$BiVO_4$ were explained considering the wider band gap for this phase. Thus, in our case, the observed photoluminescence in the visible region upon illumination with 532 nm laser points out the participation of such luminescence processes in the overall mechanism. According to previous reports, the emission bands around 318.7 and 320.1 nm could be observed in Er^{3+}-doped compounds under the pumping of 486.5 and 542.4 nm (or 548.8 nm), respectively.[29,30]

Moreover, it has been also reported that violet (405–420 nm), blue (436–442 nm) and green (525–575 nm) up-conversion luminescence were simultaneously observed upon excitation at 652 nm.[31] This way, Er^{3+}-doped t-$BiVO_4$ could improve the photoefficiency by increasing the absorbed photons.

In Fig. 6, we show the photoluminescence spectra for different Er^{3+}–$BiVO_4$ systems by excitation at 523 and 655 nm.

In the case of 523 nm excitation, the luminescence appears for Er content higher than 3 at%, as confirmed by Raman spectra. Thus, the observed emission bands match with the m-$BiVO_4$ edge. However, as for this erbium content the monoclinic phase is in a very low percentage, the emission bands appear exalted. It is worth noting that 5 at% sample exhibits the highest luminescent emission. However, this higher luminescent behaviour does not lead to a higher photocatalytic activity. It is clear that for higher Er content, a detrimental effect occurs which could be associated with the occurrence of the recombination processes. So, in spite of the higher available photons this would not be translated into effective photogenerated charges. A similar trend was observed for Y^{3+} doped $BiVO_4$ for which a decreasing photoactivity is found for doping level higher than 3 at%.[28] In contrast, for 655 nm excitation, the emission bands between 430 and 460 nm appear with much diminished intensity. This would indicate the absorption of such photons by the t-$BiVO_4$. Thus, a cooperative "up-conversion" mechanism could be envisaged. A similar effect was already observed for Er^{3+} doped TiO_2, for which an "up-conversion" mechanism would be responsible in part for the better photocatalytic behaviour.[32]

Conclusions

We have prepared highly efficient Er doped $BiVO_4$ photocatalytic systems by means of the microwave assisted hydrothermal method. The presence of Er^{3+} ions induces the appearance of the tetragonal phase at higher loading that might be incorporated into the structure by Bi^{3+} substitution. This is the first time that tetragonal $BiVO_4$ is reported to exhibit better photocatalytic performance than the monoclinic one. Such improved photoactivity of the t-$BiVO_4$ under sun-like irradiation was correlated to the occurrence of a luminescence process which takes place for such a structure. The cooperative mechanism induces an unexpected photoactivity enhancement by increasing the number of the adequate photons. This novel approach opens a wide field of applications to other photocatalytic materials having good luminescence properties as host matrix such as molybdates, tungstates or phosphates.

Acknowledgements

This work was supported by the projects *ENE2011-24412* and *P09-FQM-4570*. The authors also thank the Global Research Laboratory Program of the National Foundation of Korea funded by the Ministry of Education, Science and Technology of Korea (grant number: 2010-00339). S. Obregón thanks CSIC for the concession of a *JAE-Pre* grant. The authors also thank Dr A. I. Becerro for Rietveld refinement.

Notes and references

1 A. Kubacka, G. Colón and M. Fernández-García, *Catal. Today*, 2009, **143**, 286–292.
2 A. Kubacka, M. Fernández-García and G. Colón, *Chem. Rev.*, 2012, **112**, 1555–1614.
3 A. Kudo, K. Omori and H. Kato, *J. Am. Chem. Soc.*, 1999, **121**, 11459–11467.
4 J. Yu and A. Kudo, *Adv. Funct. Mater.*, 2006, **16**, 2163–2169.
5 Y. Sasaki, A. Iwase, H. Kato and A. Kudo, *J. Catal.*, 2008, **259**, 133–137.
6 G. Xi and J. Ye, *Chem. Commun.*, 2001, 1893–1895.
7 S. Navalón, A. Dhkshinamoorthy, M. Alvaro and H. García, *ChemSusChem*, 2013, **6**, 562–577.
8 S. Tokunaga, H. Kato and A. Kudo, *Chem. Mater.*, 2001, **13**, 4624–4628.
9 A. Zhang, J. Zhang, N. Cui, X. Tie, Y. An and L. Li, *J. Mol. Catal. A: Chem.*, 2009, **304**, 28–32.
10 G. Li, Y. Bai and W. F. Zhang, *Mater. Chem. Phys.*, 2012, **136**, 930–934.

11 Y. Liu, B. Huang, Y. Dai, X. Zhang, X. Qin, M. Jiang and M. H. Whangbo, *Catal. Commun.*, 2009, **11**, 210–213.
12 G. Li, D. Zhang and J. C. Yu, *Chem. Mater.*, 2008, **20**, 3983–3992.
13 U. M. García-Pérez, S. Sepúlveda-Guzmán and A. Martínez-de la Cruz, *Solid State Sci.*, 2012, **14**, 293–298.
14 Y. Zhang, G. Li, X. Yang, H. Yang, Z. Lu and R. Chen, *J. Alloys Compd.*, 2013, **551**, 544–550.
15 W. Wang, Q. Shang, W. Zheng, H. Yu, X. Feng, Z. Wang, Y. Zhang and G. Li, *J. Phys. Chem. C*, 2010, **114**, 13663–13669.
16 W. Qin, D. Zhang, D. Zhao, L. Wang and K. Zheng, *Chem. Commun.*, 2010, **46**, 2304–2306.
17 S. Obregón and G. Colón, *Chem. Commun.*, 2012, **48**, 7865–7867.
18 B. Yan and X. Q. Su, *J. Non-Cryst. Solids*, 2006, **352**, 3275–3279.
19 H. Liu, J. Yuan, Z. Jiang, W. Shangguan, H. Einaga and Y. Teraoka, *J. Solid State Chem.*, 2012, **186**, 70–75.
20 A. K. Bhattacharya, K. K. Mallick and A. Hartridge, *Mater. Lett.*, 1997, **30**, 7–13.
21 N. S. Singh, R. S. Ningthoujam, G. Phaomei, S. D. Singh, A. Vinud and R. K. Vatsa, *Dalton Trans.*, 2012, **41**, 4404–4412.
22 S. Obregón, A. Caballero and G. Colón, *Appl. Catal., B*, 2012, **117–118**, 59–66.
23 A. Kubacka, M. Fernández-García and G. Colón, *J. Catal.*, 2008, **254**, 272–284.
24 H. Fan, T. Jiang, H. Li, D. Wang, L. Wang, J. Zhai, D. He, P. Wang and T. Xie, *J. Phys. Chem. C*, 2012, **116**, 2425–2430.
25 K. E. Kweon and G. S. Hwang, *Phys. Rev. B: Condens. Matter*, 2013, **87**, 205202.
26 M. L. Guan, D. K. Ma, S. W. Hu, Y. J. Chen and S. M. Huang, *Inorg. Chem.*, 2010, **50**, 800–805.
27 G. Tan, L. Zhang, H. Ren, S. Wei, J. Huang and A. Xia, *ACS Appl. Mater. Interfaces*, 2013, **5**, 5186–5193.
28 S. Usai, S. Obregón, A. I. Becerro and G. Colón, submitted.
29 N. Zu, Z. Yang and Z. Dai, *Physica B*, 2008, **403**, 174–177.
30 H. Xu and Z. Jiang, *Chem. Phys.*, 2003, **287**, 155–159.
31 H. Yang, Z. Dai and Z. Sun, *J. Lumin.*, 2007, **124**, 207–212.
32 S. Obregón, A. Kubacka, M. Fernández-García and G. Colón, *J. Catal.*, 2013, **299**, 298–306.